JACS
JOURNAL OF THE AMERICAN CHEMICAL SOCIETY

Article

pubs.acs.org/JACS

Tunable Morphology of the Self-Assembled Organic Microcrystals for the Efficient Laser Optical Resonator by Molecular Modulation

Xuedong Wang,[†,‡] Hui Li,[†,‡] Yishi Wu,[†] Zhenzhen Xu,[§] and Hongbing Fu*[,†,§]

[†]Beijing National Laboratory for Molecular Sciences (BNLMS), Institute of Chemistry, Chinese Academy of Sciences, Beijing 100190, P. R. China

[‡]Graduate University of Chinese Academy of Sciences, Beijing 100049, P. R. China

[§]Department of Chemistry, Capital Normal University, Beijing 100048, P. R. China

Supporting Information

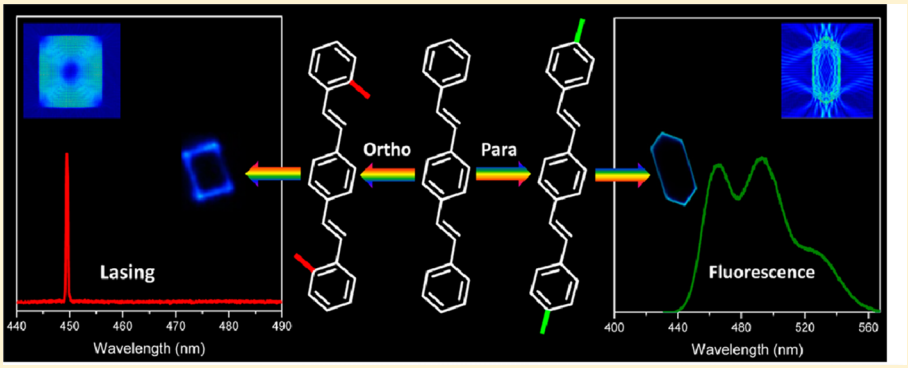

ABSTRACT: Organic single-crystalline micro/nanostructures can effectively generate and carry photons due to their smooth morphologies, high photoluminescence quantum efficiency, and minimized defects density and therefore are potentially ideal building blocks for the optical circuits in the next generation of miniaturized optoelectronics. However, the tailor-made organic molecules can be generally obtained by organic synthesis, ensuring that the organic molecules aggregate in a specific form and generate micro/nanostructures with desirable morphology and therefore act as the efficient laser optical resonator remains a great challenge. Here, the molecular modulation of the morphology on the laser optical resonator properties has been investigated through the preparation of the elongated hexagonal microplates (PHMs) and the rectangular microplates (ORMs), respectively, from two model isomeric organic molecules of 1,4-bis(4-methylstyryl)benzene (*p*-MSB) and 1,4-bis(2-methylstyryl)benzene (*o*-MSB). Significantly, fluorescence resonance phenomenon was only observed in the individual ORM other than the PHM. It indicates that the rectangular resonators possess better light-confinement property over the elongated hexagonal resonators. More importantly, optically pumped lasing action was observed in the *o*-MSB rectangular morphology microplates resonator with a high $Q \approx 1500$ above a threshold of ~540 nJ/cm^2. The excellent optical properties of these microstructures are associated with the morphology, which can be precisely modulated by the organic molecular structure. These self-assembled organic microplates with different morphologies can contribute to the distinct functionality of photonics elements in the integrated optical circuits at micro/nanoscale.

INTRODUCTION

The morphology of the semiconductor micro/nanostructures precisely lies at the heart of the physical and the chemical properties of the functional micro/nanomaterials.[1−5] For instance, M. A. EI-Sayed and co-workers demonstrated that Pt nanoparticles of different morphologies have different facets, which further led to the different catalytic activities for the same chemical reaction.[6] More significantly, the Ag nanocrystals with controlled morphologies have contributed to a distinguished discovery of morphology-dependent and size-dependent plasmon resonance.[7−9] As is indicated, the performance of these optoelectronic devices is attributed with the morphology of these micro/nanoscale fabricated structures. As compared with the inorganic/metal counterparts, small organic molecules are attractive photonic and electronic materials because of their tailor-made molecular structure, tunable optical properties, and compatibility with plastic substrates.[10] Especially the organic single-crystalline micro/nanostructures can effectively carry photons and electrons due to their perfect molecular arrangements, minimized defects, and eliminated grain boundaries in crystals[11] and therefore are potentially ideal building blocks for the miniaturized optoelectronics devices.[12−16] Accordingly, highly ordered molecule packing mode is formed within the organic single-crystalline micro/nanocrystals, resulting in anisotropic charge transport in field effect

Received: August 27, 2014
Published: November 4, 2014

   dx.doi.org/10.1021/ja5088503 | *J. Am. Chem. Soc.* 2014, 136, 16602−16608

transistors.[17] What's more, the single-crystalline organic micro/nanostructures with regular morphology have been demonstrated for the active media and the optical resonators simultaneously for the laser applications.[18−20] However, the controlled synthesis of organic micro/nanostructures with desirable morphologies has not been fully realized.[21]

As we all know, organic single-crystalline structures fabricated from organic molecules are based on the intermolecular interaction, such as van der Waals' force, ca. 5 kJ/mol. It is totally different from the strong bonding interaction, such as ionic bonding, ca. 200 kJ/mol, within the inorganic crystals. Thus, the outer environment including the kinds of solvents, temperature, solution concentration, and surfactants can easily affect the nucleation of organic micro/nanocrystals. For the single organic molecule, these influencing factors are so numerous and sophisticated that the aim of organic micro/nanostructures with controlled morphology is not easy to reach.[22,23] It is noted that the flexibility in the organic molecule synthesis and modification make them useful for the construction of various micro/nanostructures. Moreover, the morphology−property relationship of organic micro/nanostructures has not been explored.[24]

Here, we take the 'molecular modulation' approach to obtain the various morphologies of organic micro/nanostructures for the efficient laser optical microresonators. The organic molecules used in our study are the *p*-distyrylbenzene (DSB) derivatives 1,4-bis(2-methylstyryl)benzene (*o*-MSB) and 1,4-bis(4-methylstyryl)benzene (*p*-MSB), which have been demonstrated for the excellent amplified spontaneous emission (ASE) characteristics.[25] The *p*-MSB elongated hexagonal microplates (PHMs) and *o*-MSB rectangular microplates (ORMs) from these two model π-conjugated isomeric organic molecules have been fabricated by a facile bottom-up method.[26−29] Importantly, fluorescence resonance phenomenon was observed in the individual ORM other than PHM. It indicates that the as-prepared *o*-MSB microplates with rectangular morphology possess better light-confinement property and higher quality (Q) factors over the *p*-MSB microplates with elongated hexagonal morphology. Furthermore, optically pumped lasing action was only observed in the *o*-MSB rectangular microplate resonator with a high-quality factor ($Q \approx 1500$) above a threshold of ~540 nJ/cm^2. More significantly, by decreasing the size of *o*-MSB microplates, single-mode lasing was successfully achieved in the ORMs with small size (i.e., edge lengths l_1 = 2.0 μm, and l_2 = 1.8 μm). These self-assembled organic single-crystalline microplates with various morphologies are realized by molecular modulation, which open up the distinct functionality of organic photonics in the integrated optical circuits.

EXPERIMENTAL SECTION

Materials. The compounds of 1,4-bis(2-methylstyryl)benzene (*o*-MSB) and 1,4-bis(4-methylstyryl)benzene (*p*-MSB) were purchased from Sigma-Aldrich and were used without further treatment. The solvent of carbondisulfide (CS_2, HPLC grade) was purchased from Beijing Chemical Agent Ltd., China, and was used without further treatment.

Preparation of Organic Microplates. In a typical synthesis, 2 mg of *p*-MSB (*o*-MSB) was completely dissolved in 10 mL of CS_2 at room temperature, and then the solution was dropped onto the quartz substrate. Finally the solvents evaporated, and the microstructures were obtained in a large scale.

Structure Characterization. TEM measurement was performed at room temperature at an accelerating voltage of 100 kV. Fluorescence images were recorded using an Olympus research inverted system microscope (FV1000-IX81, Tokyo, Japan) equipped with a charge couple device (CCD, Olympus DP71, Tokyo, Japan) camera. The excitation source is a mercury lamp equipped with a band-pass filter (330−380 nm for UV-light). The samples were prepared by placing a drop of solution onto a cleaned quartz plate.

Micro-PL (μ-PL) Setup. The single-particle spectroscopy was performed by using a homemade optical microscope equipped with a 50 × 0.9 NA objective (Supporting Information, Figure S4). The second harmonic (λ = 400 nm, pulse width 150 fs) of a 1 kHz Ti:sapphire regenerative amplifier was amplified to a 50 μm diameter spot to uniformly excite the selected isolated microcrystal on a 2D movable table. The spatially resolved PL spectra from single microplate were collected underneath using a 3D-movable 100 × 0.9 NA objective with a spatial resolution <1 μm. A 420 nm long-wave pass dielectric filter was used to block any scattered excitation light. Finally the collected PL was coupled to an optical fiber with diameter 25/125 μm (core/cladding) and detected using a liquid-nitrogen-cooled CCD (SPEC-10-400B/LbN, Roper Scientific) attached to a polychromator (Spectropro-550i, Acton). This setup allows us to characterize single microplate and avoid the influence of other plates in the excitation area.

RESULTS AND DISCUSSION

Figure 1A shows the chemical structure of these two model isomeric π-conjugated small organic molecules 1,4-bis(4-methylstyryl)benzene (*p*-MSB) and 1,4-bis(2-methylstyryl)-benzene (*o*-MSB), which are the simplified derivatives of *p*-distyrylbenzene (DSB). To know the molecular modulation of the crystal morphology based on the organic molecules, we first simulated the growth morphology of *p*-MSB and *o*-MSB crystals based on the attachment energies using the Materials

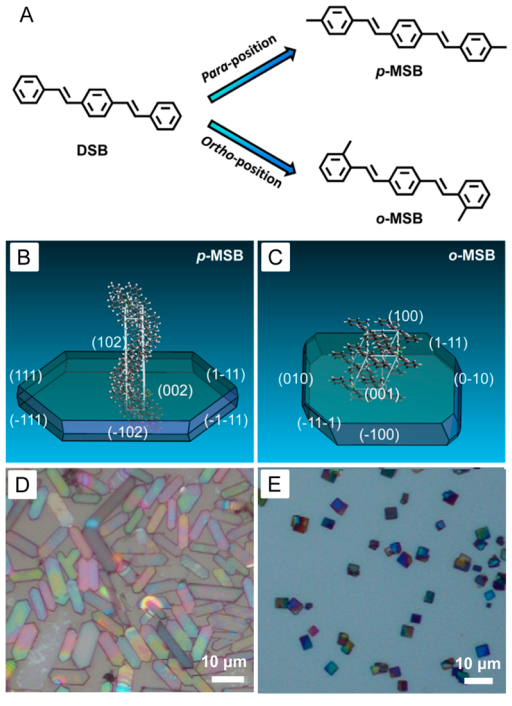

Figure 1. (A) Two model isomeric π-conjugated organic molecules *p*-MSB and *o*-MSB derivatives of DSB. (B) The simulated growth morphology of *p*-MSB molecules based on the attachment energies. (C) The simulated growth morphology of *o*-MSB molecules based on the attachment energies. (D) The bright optical image of the PHMs in a large scale. (E) The bright optical images of the as-prepared ORMs in a large scale. The scale bars are both 10 μm.

dx.doi.org/10.1021/ja5088503 | J. Am. Chem. Soc. 2014, 136, 16602−16608

Studio package.[30] From the calculated results, the growth morphology of *p*-MSB molecules is predicted as the elongated hexagonal plate-like structure (Figure 1B). In contrast with *p*-MSB, *o*-MSB molecules are prone to form the rectangular plate-like structure, as shown in Figure 1C.

In experiment, microstructures of *p*-MSB and *o*-MSB were prepared by a facile solution-drying method at room temperature.[26] Significantly, consistent with the above predicted growth morphology of *p*-MSB crystal, the as-prepared PHMs are revealed in Figure 1D. The flatness of the facets and the elongated hexagonal shape of PHMs are clearly shown in the atomic force microscopy (AFM) image (Figure 2A). Combined

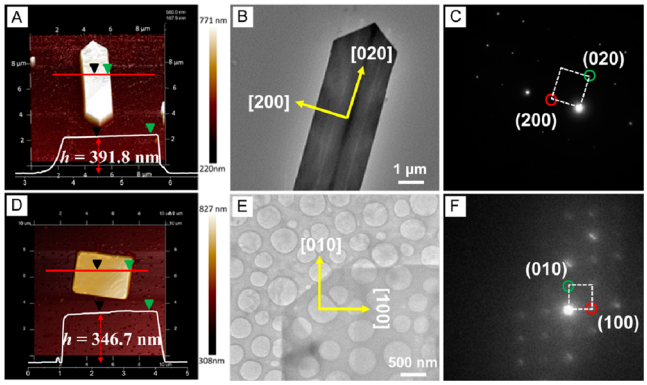

Figure 2. (A) AFM image of one PHM and height profile (bottom inset) along the red line in the image. (B) TEM image of one sample PHM. Scale bar is 1 μm. (C) The corresponding SAED pattern of this PHM in (B). (D) AFM image of one ORM and height profile (bottom inset) along the red line in the image. (E) TEM image of one sample ORM. Scale bar is 500 nm. (F) The corresponding SAED pattern of this ORM in (E).

with the height profile along the red line in the AFM image (the bottom inset of Figure 2A), it is confirmed that the PHMs have the height (*h*) of ∼400 nm. Furthermore, the TEM image (Figure 2B) and the selected area electron diffraction (SAED, Figure 2C) results proclaim that the elongated hexagonal single-crystalline microplate growing along the [020] crystal direction is superior to growing along the [200] crystal direction. The coincident X-ray diffraction (XRD) pattern of the microcrystals shown in the bottom panel of Figure S1 (Supporting Information) reveals that all the reflections can be attributed to the (002)s crystal planes.

As compared with *p*-MSB, the *o*-MSB molecules are aggregated into the rectangular microplates as shown in Figure 1E. The TEM image (Figure 2E) and the corresponding SAED (Figure 2F) results demonstrate that the two prominent growth directions of the ORMs are [100] and [010] crystal directions. This agrees with the XRD measurements (Supporting Information, Figure S1), in which all reflections can be attributed to the (001)s crystal planes. Figure 2D shows the AFM image and the height file of one typical ORM, which shows regular shape with thickness of ∼350 nm. In the comparison between these two molecule structures of *o*-MSB and *p*-MSB, we can find that their difference is only the position of the methyl substituent on the molecular backbone of DSB. According to the above-predicted growth morphology of *p*-MSB molecules, the calculated attachment E_{att} (*hkl*) of various crystal faces (*hkl*) follows the order: $E_{att}(002)s > E_{att}(122)s > E_{att}(111)s$ (Supporting Information, Table S2). Correspondingly, the (002) and (00-2) planes has the largest exposed facet area percentage (∼72.38%). It is consistent with the observed flat top/bottom facets, which are bounded by (002) crystal planes in experiment (Supporting Information, Figure S1). This agreement is also established for the ORM (Supporting Information, Figure S1 and Table S2). Thus, the simulated and experimental results both presented that the position of methyl can modulate the morphology of organic microcrystals. What's more, from our previous research, it has been demonstrated that the DSB molecules themselves can aggregate into the equilateral hexagonal microplates.[18] As is indicated, these organic molecules with slight difference can effectively contribute to the distinctive morphologies of these microstructures. In a short conclusion, these above-discussed results illustrate that the molecular structure of these π-conjugated organic compounds can remarkably modulate the morphology of the self-assembled organic single-crystalline microstructures.

Interestingly, Figure 3A shows the microscopy fluorescence image of these as-prepared PHMs, which exhibited intense pale

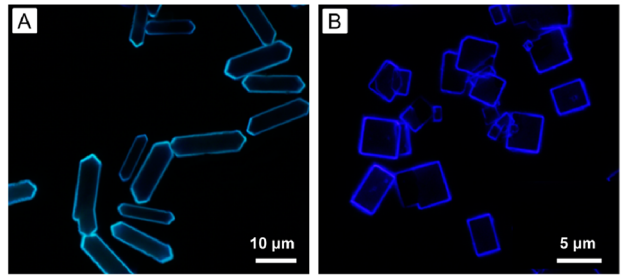

Figure 3. (A) Fluorescence microscopy image of the as-prepared PHMs excited with UV band (330−380 nm) from a mercury lamp. Scale bar is 10 μm. (B) Fluorescence microscopy image of the as-prepared ORMs excited with UV band from a mercury lamp. Scale bar is 5 μm.

blue emission with the optical wave guiding characteristic under the excitation of UV band (330−380 nm) from a mercury lamp. From the observation of Figure 3B, the bright pale blue edges and blackbody of the as-prepared ORMs are also observed. Furthermore, the fluorescent polarization studies (polarization-dependent PL, Supporting Information, Figures S5 and S6) of these two microplates both show that the PL intensity oscillates with a period of 180°.[31,32] This oscillatory manner should be a direct consequence of the diverse molecular transition dipole moment orientations within these two kinds of organic microplates. It should be noted that the single-crystalline organic microcrystals with regular shapes can serve as the active medium of emission and the optical microresonator feedback simultaneously.[18,19]

Room-temperature lasing action was achieved in the individual *o*-MSB rectangular microplate; meanwhile only spontaneous fluorescence emission was observed in the single elongated hexagonal *p*-MSB microplate. The dependence of PL spectra on the pump density (obtained from one sample PHM shown in the inset) is indicated in Figure 4A. We can only observe that the PL intensity increases as the pump density enhancing from 300 to 1150 nJ/cm^2. Moreover, the lasing action was detected neither at 0-1 nor 0-2 peaks until the morphology of the PHM suffered damages under the increasing optical excitation. Consistent with it, the change of integrated intensities at 0-1 peak as a function of excitation intensity is exhibited in Figure 4C where the intensity dependence is fitted to a power law x^p with $p = 0.51 \pm 0.03$, demonstrating a

dx.doi.org/10.1021/ja5088503 | J. Am. Chem. Soc. 2014, 136, 16602−16608

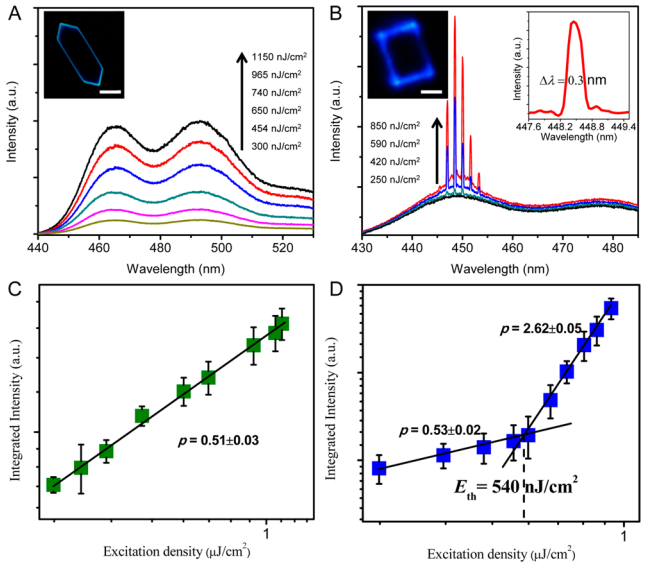

Figure 4. (A) PL spectra obtained from one typical elongated hexagonal *p*-MSB microplate excited at different energies (300, 454, 650, 740, 965, and 1150 nJ/cm^2) at room temperature. Inset: the fluorescence microscopy image of this PHM. Scale bar is 2 μm. (B) PL spectra obtained from *o*-MSB rectangular microplate excited at different energies (250, 420, 590, and 850 nJ/cm^2) at room temperature. Left inset: the fluorescence microscopy image of this ORM. Scale bar is 5 μm. Right inset: the $\Delta\lambda$ (0.3 nm) is the line-width of the peak around 448 nm. $Q = \lambda/\Delta\lambda$ = 440 nm/0.3 nm ≈ 1500. (C) PL integrated area of the 0-1 peak (around 460 nm) as a function of the pump densities for *p*-MSB microplate. (D) PL integrated area of the 0-1 peak (around 450 nm) as a function of the pump densities for *o*-MSB microplate. The lasing threshold is identified as the intersection between the sublinear and the superlinear regions.

remains in the sublinear regime (exciton−exciton annihilation).[33] In sharp contrast, the laser emission obtained from one ORM is shown in Figure 4B. At lower pump density of 250 nJ/cm^2, the PL spectrum consists with a broad spontaneous emission (the black curve). With the pump density increasing from 420 to 850 nJ/cm^2, the lasing action becomes more and more obvious. We can distinctly see a set of sharp peaks developing on the top of the 0-1 transition which reveals the strong laser emission. This coincides with Figure 4D where the threshold can be clearly observed at 540 nJ/cm^2.

Below the lasing threshold, the integrated intensity depends sublinearly on the excitation density with $p = 0.53 \pm 0.02$, which can be attributed to the bimolecular quenching (exciton−exciton annihilation). Nevertheless, a superlinear region is found above the lasing threshold with $p = 2.62 \pm 0.05$. To further verify this lasing action within the ORM, we investigated the PL lifetimes with a streak camera (Supporting Information, Figure S7). The individual ORM PL follows single exponential decay with $\tau = 2.81 \pm 0.03$ ns at a very low excitation density of $0.12E_{th}$. Upon increasing the pump intensity to $0.35E_{th}$, bi-exponential PL decay takes place with the short component ascribed to the presence of bimolecular quenching. Above the threshold, for example, at $1.83E_{th}$, the PL decay time always collapses to <10 ps and is limited by the resolution of our apparatus. This short PL lifetime above the threshold suggests the process of lasing action occurs in the ORM. The right inset of Figure 4B presents the zoomed spectrum around 448 nm, which clearly shows the $\Delta\lambda$ (a full width at half-maximum) is as small as 0.3 nm. The *Q* factor is an important parameter to describe a laser cavity. From the experiment, the *Q* factor is estimated to be as high as ∼1500 according to the definition $Q = \lambda/\Delta\lambda$, where λ is the peak wavelength and $\Delta\lambda$ is the line-width of the peak, respectively. This indicates that the high-*Q* resonant mode is formed within the *o*-MSB rectangular single-crystalline resonators.

In comparison of these two organic single-crystalline microplates with different morphologies, the ORMs successfully act as the active laser media and the optical resonator feedback for the lasing oscillator. However, only spontaneous fluorescence emission was observed, and no lasing oscillator was formed within the PHMs. As we all know, three key factors for the laser operation are the active media, the efficient optical resonator, and the source of excitation, respectively. Among them, the source of optical excitation is the same in this study. The photophysical properties of these two active media are shown in Table 1. From the table, it is shown that the *p*-MSB and *o*-MSB both have been demonstrated for the ASE, which indicates that these two organic materials both can serve as the active laser media.[25] Thus, the prominent difference between these two kinds of organic single-crystalline microplates is their morphology of the optical resonator: the elongated hexagonal shape and the rectangular shape.

Table 1. Photophysical Properties of *p*-MSB and *o*-MSB Microcrystals

crystal	Φ (%)	τ (ns)	k_F (ns^{-1})^a	E_{ASE} (μJ cm^{-2})^b
p-MSB	89 ± 1	2.51 ± 0.2	0.36 ± 0.1	25 ± 5
o-MSB	90 ± 1	2.84 ± 0.2	0.32 ± 0.1	14 ± 2

^{a}The radiative decay rate calculated according to $k_F = \Phi/\tau$. ^{b}ASE characteristics of the single crystals.

To make a laser, however, it is not enough with the laser active materials. The lasers must have a positive resonator feedback with high *Q* factors allowing for the generation of light. The photons go back and forth within the resonator, each time provoking appearance of the new photons in the same quantum state. From these results, we conjecture that the morphology of these microstructures can be the reason for the above-observed laser action in the ORM with rectangular morphology other than PHM with elongated hexagonal morphology.[18,34] Therefore, the morphology of these as-prepared microstructures plays a vital role in the resonator properties of these fabricated laser devices. Moreover, the molecular structure can easily modulate the morphology of these self-assembled single-crystalline micro/nanostructures.

In order to clarify the resonator phenomena of these organic single-crystalline microplates, spatially resolved spectra were collected. Figure 5A presents the spectrum (gray line) from the body of the ORM, and a typical PL spectrum (blue line) obtained from the edge emission of one sample ORM. More impressively, periodic intensity variations were observed in edge emission spectrum of the individual rectangular microplate. Such variations were never apparent in body spectrum, suggesting that they were due to the optical resonator resonances. Furthermore, the μ-PL of microplates with different sizes are shown in Figure S8 (Supporting Information). We can find that microplates with larger size have more resonance peaks on the PL spectra. This fluorescence resonance phenomenon should be ascribed to some appropriate cavity feedback, such as a FP-mode cavity and WGM cavity. Significantly, our self-assembled rectangular microplates can

dx.doi.org/10.1021/ja5088503 | J. Am. Chem. Soc. 2014, 136, 16602−16608

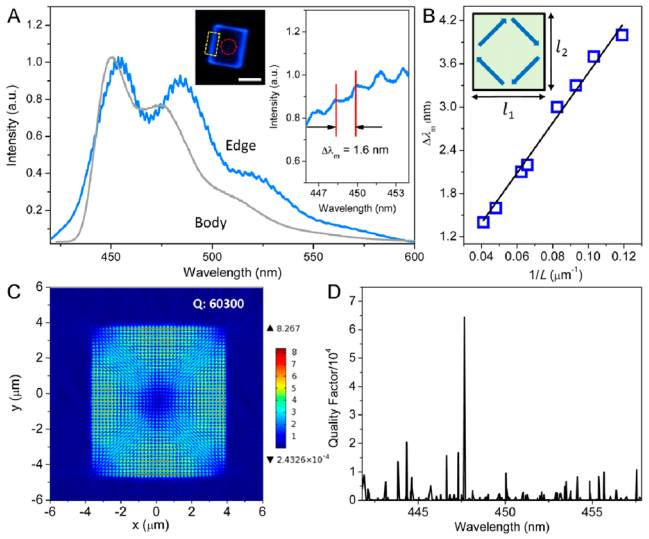

Figure 5. (A) μ-PL spectra of one single ORM. Top inset: the PL microscopy image of the sample ORM, the yellow square rectangular line denotes the edge region, and the red circle dashed line denotes the body region. Scale bar is 5 μm. Emission spectra collected from the edge region (blue line) and body region (gray line) of this isolated *o*-MSB rectangular microplate. Right inset: the magnification of spectrum around 450 nm. (B) The mode spacing $\Delta\lambda_m$ at 450 nm (0-1) and $1/L$ of the resonator, showing clearly a linear relationship. Inset: schematic picture of the light-path of the 4-WGM in the rectangular resonator. (C) Simulated 2D normalized electric field (surface: electric field norm (V/m), λ = 450 nm, n = 1.80) of the *o*-MSB rectangular resonator. (D) Simulated 2D normalized electric field (surface: electric field norm (V/m), λ = 450 nm, n = 1.80) of the *p*-MSB elongated hexagonal resonator.

simultaneously act as the active medium of laser emission and the optical resonator feedback. To form a stable oscillator in the resonator and make light waves strengthened due to interference, the phase change for the light going a round trip in the resonator should be an integer of 2π, i.e., the resonance condition:

$$nL = m\lambda \tag{1}$$

where n, L are the phase refractive index of the crystal and round-trip distance, respectively, and m is the order of the mode (an integer). Restricted by the condition, only certain frequencies of light are ultimately chosen and enhanced by the optical resonator. Thus, a set of sharp peaks with certain frequencies was observed in the PL spectra of ORNs. For the FP-mode cavity, it can be formed either by the top and bottom rectangular facets (Supporting Information, Figure S9A) or by two opposing edge facets of ORM (Figure S9B).[35,36]

This ORM resonator can also support 4-WGM (the left inset of Figure 5B), where the light is totally reflected by the four lateral sides of the rectangular microplate.[18] The zoomed spectrum (from 446 to 454 nm) shows the distance between two adjacent peaks around 450 nm is 1.6 nm (the right inset of Figure 5A), which is as the definition of mode spacing $\Delta\lambda_m$. Further $\Delta\lambda_m$ can be expressed as eq 2:

$$\Delta\lambda_m = \frac{\lambda^2}{L[n - \lambda(dn/d\lambda)]} \tag{2}$$

where n is the phase refractive index of the crystal (n = 1.8), L is the round-trip distance of a cavity mode, $dn/d\lambda$ is the dispersion relation. The round-trip distance L within the 4-WGM resonators could be defined as the following expression:

$$L = 2\sqrt{l_1^2 + l_2^2} \tag{3}$$

where l_1 and l_2 are the edge lengths of the rectangular microplates. Figure 5B presents a plot of the mode spacing $\Delta\lambda_m$ at λ of ~450 nm versus $1/L$ within the 4-WGM cavity, demonstrating clearly a linear relationship. This linear relationship is consistent with that the light travels in the form of 4-WGM rather than other forms in the rectangular resonator.[37] To further know the mechanism of the cavity mode within the ORM, the electromagnetic field distribution of the rectangular resonator was simulated, as shown in Figure 5C. The calculated result presents that the *o*-MSB rectangular resonator provides excellent confinement for the electromagnetic field. Furthermore, we calculated the quality (Q) factors corresponding to this ORM resonator. Figure 5D shows that there exist several high-Q modes (~20000) in the ORM. These high-Q modes can explain the above-observed WGM laser in the ORMs.

As mentioned above, the ORMs with rectangular morphology can provide multimode lasing. As compared with multimode lasing, single-mode lasing has its inherent merits as excellent monochrome properties of laser beam, fine optical coherence, and good stability of laser oscillation due to the absent of mode competition. In principle, the gain of lasing action is determined by the spatial spectra and the spectral overlap between the resonance and the gain material.[38] It also means that smaller resonator provides less resonance states. In experiment, Figure 6A presents the three lasing spectra

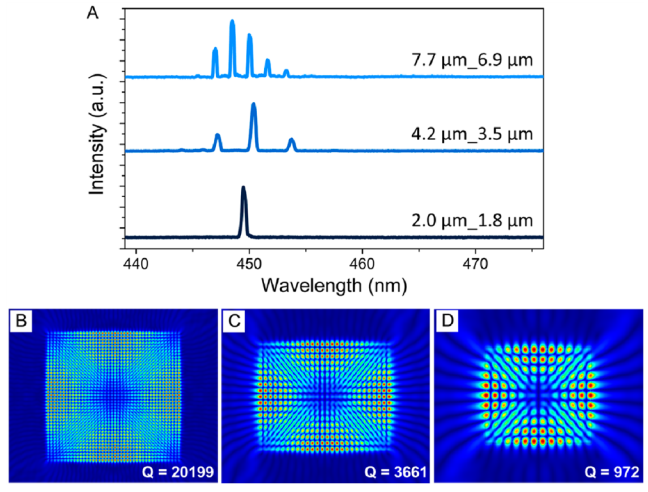

Figure 6. (A) Laser spectra of three rectangular microplates with different sizes (l_1 = 7.7 μm, l_2 = 6.9 μm; l_1 = 4.2 μm, l_2 = 3.5 μm; and l_1 = 2.0 μm, l_2 = 1.8 μm). (B–D) Simulated 2D normalized electric field (λ = 450 nm, n = 1.80) in the plane of these three corresponding microplates resonators. The ORMs with different sizes can all provide the efficient WGM optical resonators for lasing oscillator. Red corresponds to the highest field density, and blue is the lowest field density.

sequentially from top to bottom, from three sample ORMs with sizes varying from l_1 = 7.7 μm, l_2 = 6.9 μm; to l_1 = 4.2 μm, l_2 = 3.5 μm; and to l_1 = 2.0 μm, l_2 = 1.8 μm. It should be noted here that the lasing spectra are collected from the whole microplate. Under high optical excitation density above the lasing threshold, such as $3.5E_{th}$, the lasing mode (or stimulated emission) completely dominates the PL spectrum, while the

dx.doi.org/10.1021/ja5088503 | J. Am. Chem. Soc. 2014, 136, 16602–16608

spontaneous emission remains at low intensity. Thus, as seen from Figure 6A, only lasing resonance peaks are observed in the PL spectra. As in the ORM with small size (l_1 = 2.0 μm, l_2 = 1.8 μm), single-mode lasing was successfully achieved at room temperature. It is that the single-crystalline nature of these microplates contributes to the high density of optical gain, which can account for the observed laser action within ORM with such small size. Figure 6B−D demonstrates the simulated electromagnetic distribution of these three corresponding ORMs resonators. The simulation results indicate that the ORMs with different sizes can all act as the efficient WGM optical resonators for lasing oscillator.

In practice, these as-prepared ORMs are not absolutely uniform. As indicated in Figure S9 (Supporting Information), the quality factors Q of these rectangular geometries (square resonators or rectangular resonators) are all larger than 1500, which promises the efficient optical resonator for the laser operation. Among these geometries, the square ORM resonator has the largest Q of ~6700. Moreover, the simulated electric field distribution of square optical resonator (such as edge lengths l_1 = 4 um, and l_2 = 4 um) shows the excellent light confinement. Meanwhile, the rectangular microplates (such as l_1 = 5 um, and l_2 = 3 um) can still confine the electric field in the rectangular optical resonator. Thus, the *o*-MSB rectangular microplates (ORMs) can all provide the efficient optical resonator for laser operation.

In a sharp contrast, a μ-PL spectrum (red line) of the edge emission of the individual PHM shows no resonance phenomenon as the PL spectrum (green line) of the body has (Figure 7A). It illustrates that the PHM cannot act as an efficient optical resonator. To further know the light-confinement properties in individual PHM, we simulated the electromagnetic field distribution of the hexagonal resonators with different morphologies (Figure 7B). The right top inset of Figure 7B shows that d_1 and d_2 are the long edge and the short edge of the elongated hexagonal microplates, respectively. The d_1/d_2 is defined as the ratio η, and the sum of d_1 and d_2 is defined as a constant value of 10 μm. The calculated Q of the optical resonator versus the ratio η is plotted in Figure 7B. As we can see, the Q factor decreases dramatically with the increasing value of η. When η = 1, the resonator is the equilateral hexagonal resonator. This regular hexagonal resonator indeed provides the excellent light confinement with the high-Q mode of ~2500, as indicated by the electric field distribution (left top inset of Figure 7B). This simulated high-Q mode is also consistent with our previous observation of WGM microlaser within the DSB equilateral hexagonal microdisks.[18] Again the resonator with high-Q has been demonstrated for the operation of lasing oscillator.

In the case of PHMs with elongated hexagonal morphology (η = 3, red circle), the bottom inset of Figure 7B demonstrates that the electromagnetic field distribution both exists within the hexagonal resonator and in the surroundings, which means poor light confinement in this PHM resonator with low-Q modes ($Q \approx 100$) by simulation. As is known to us, higher Q indicates a lower rate of energy loss relative to the stored energy of the resonator and the oscillations die out more slowly.[32] It also means that high-Q resonator provides the effective platform for the laser action. Thus, the elongated hexagonal morphology accounts for the low-Q modes and the absence of laser action in the individual PHMs. As compared with PHMs, the ORMs with rectangular morphology inherently have the high-Q modes, which hold the promise for the laser action. In a short conclusion, the light-confinement property (Q) can be attributed with the morphology of these self-assembled single-crystalline organic microstructures. More importantly, the morphology of these microstructures can be precisely modulated by the organic molecular structure.

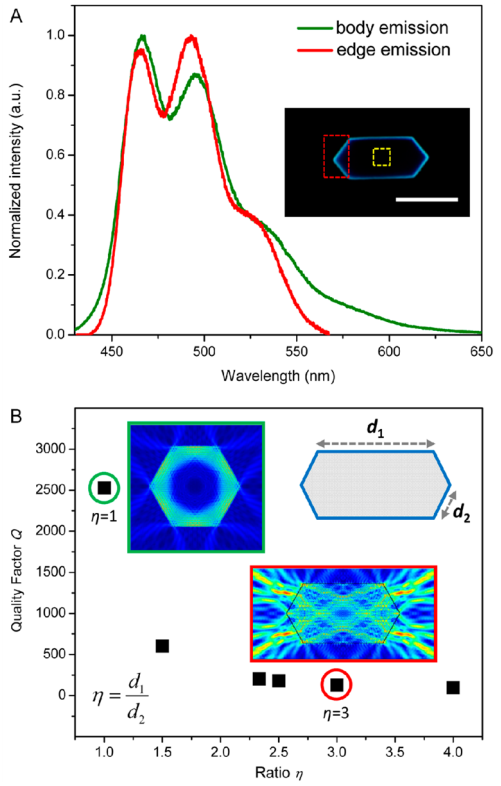

Figure 7. (A) μ-PL spectra of one typical PHM. Right inset: red rectangular dashed line denotes the edge region, and the yellow square dashed line denotes the body region. Scale bar is 5 μm. PL spectra collected from the edge (red line) and body (green line) of an isolated PHM. (B) Quality factors Q dependence of the shape of the elongated hexagonal microplate. Right top inset: d_1 and d_2 are the long edge and the short edge of the elongated hexagonal microplate, respectively. The ratio η is defined as d_1/d_2, and the sum of d_1 and d_2 equals a constant value of 10 μm. Left top inset: simulated 2D normalized electric field (surface: electric field norm (V/m), λ = 460 nm, n = 1.80) of the normal hexagonal resonator corresponding to the η = 1 (denoted by the green circle). Bottom inset: simulated 2D normalized electric field (surface: electric field norm (V/m), λ = 460 nm, n = 1.80) of elongated *p*-MSB hexagonal resonator corresponding to the η = 3 (denoted by the red circle) in the case of PHMs. Red corresponds to the highest field density, and blue is the lowest field density.

■ CONCLUSION

In summary, the molecular modulation of the morphology on the organic optical microresonator properties has been investigated through the preparation of elongated hexagonal microplates and rectangular microplates from two model isomeric molecules of 1,4-bis(4-methylstyryl)benzene (*p*-MSB) and 1,4-bis(2-methylstyryl)benzene (*o*-MSB), respectively. Impressively, fluorescence resonance phenomenon was observed in the individual *o*-MSB rectangular microplate (ORM) rather than the *p*-MSB elongated hexagonal microplate (PHM). It indicates that the ORMs with rectangular morphology possess better light-confinement property and higher quality (Q) factors over the PHMs with elongated hexagonal morphology. More significantly, optically pumped

dx.doi.org/10.1021/ja5088503 | J. Am. Chem. Soc. 2014, 136, 16602−16608

lasing action was only observed in the ORM with a high quality factor Q of ~1500 above a lasing threshold of ~540 nJ/cm^2. By decreasing the size of ORMs, single-mode lasing was successfully achieved in the ORMs with small size (i.e., edge lengths l_1 = 2.0 μm, and l_2 = 1.8 μm). Thus, the molecule–morphology–property relationship was successfully established for these self-assembled organic single-crystalline microplates. These self-assembled organic microplates with different morphologies are natural light sources with distinctive properties, which could be integrated on the optics chip at micro/nanoscale.

■ ASSOCIATED CONTENT

Supporting Information

XRD patterns of the as-prepared microstructures; crystallographic data of the single crystals; the calculated attachment energies E_{att} of various crystal facets; schematic illustration of the near-field scanning optical microscopy; absorption and fluorescence spectra; μ-PL spectra of ORMs with different sizes; fluorescence delay files; fluorescent polarization study of microplates; the schematic pictures of two kinds of FP-mode cavity; and the shape-dependent quality factors of ORMs. This material is available free of charge via the Internet at http://pubs.acs.org/.

■ AUTHOR INFORMATION

Corresponding Author

hongbing.fu@iccas.ac.cn

Notes

The authors declare no competing financial interest.

■ ACKNOWLEDGMENTS

This work was supported by the National Natural Science Foundation of China (nos. 21073200, 21273251, 91333111, 21190034, 21221002), Beijing Municipal Science & Technology Commission (no. Z131103002813097), project of Construction of Innovative Teams and Teacher Career Development for Universities and Colleges Under Beijing Municipality (IDHT20140512), the National Basic Research Program of China (973) 2011CB808402, 2013CB933500, and the Chinese Academy of Sciences.

■ REFERENCES

(1) Choi, H. C.; Park, J. E.; Park, C. *Acc. Chem. Res.* **2014**, *47*, 2353.
(2) Senyuk, B.; Evans, J. S.; Ackerman, P. J.; Lee, T.; Manna, P.; Vigderman, L.; Zubarev, E. R.; van de Lagemaat, J.; Smalyukh, I. I. *Nano Lett.* **2012**, *12*, 955.
(3) Chandrasekhar, N.; Chandrasekar, R. *Angew. Chem., Int. Ed.* **2012**, *51*, 3556.
(4) Aslam, F.; von Ferber, C. *Chem. Phys.* **2009**, *362*, 114.
(5) Ray, P. C. *Chem. Rev.* **2010**, *110*, 5332.
(6) Narayanan, R.; El-Sayed, M. A. *Nano Lett.* **2004**, *4*, 1343.
(7) Orendorff, C. J.; Sau, T. K.; Murphy, C. J. *Small* **2006**, *2*, 636.
(8) Jin, R.; Cao, Y.; Mirkin, C. A.; Kelly, K. L.; Schatz, G. C.; Zheng, J. G. *Science* **2001**, *294*, 1901.
(9) Nehl, C. L.; Hafner, J. H. *J. Mater. Chem.* **2008**, *18*, 2415.
(10) Clark, J.; Lanzani, G. *Nat. Photonics* **2010**, *4*, 438.
(11) Zhao, Y. S.; Fu, H. B.; Peng, A. D.; Ma, Y.; Liao, Q.; Yao, J. N. *Acc. Chem. Res.* **2010**, *43*, 409.
(12) An, B. K.; Gihm, S. H.; Chung, J. W.; Park, C. R.; Kwon, S. K.; Park, S. Y. *J. Am. Chem. Soc.* **2009**, *131*, 3950.
(13) Takazawa, K.; Inoue, J.-i.; Mitsuishi, K.; Takamasu, T. *Phys. Rev. Lett.* **2010**, *105*, 067401.
(14) Kong, Q.; Liao, Q.; Xu, Z.; Wang, X.; Yao, J.; Fu, H. *J. Am. Chem. Soc.* **2014**, *136*, 2382.
(15) Wang, X.; Liao, Q.; Xu, Z.; Wu, Y.; Wei, L.; Lu, X.; Fu, H. *ACS Photonics* **2014**, *1*, 413.
(16) Zhao, Y.; Peng, A.; Fu, H.; Ma, Y.; Yao, J. *Adv. Mater.* **2008**, *20*, 1661.
(17) Sundar, V. C.; Zaumseil, J.; Podzorov, V.; Menard, E.; Willett, R. L.; Someya, T.; Gershenson, M. E.; Rogers, J. A. *Science* **2004**, *303*, 1644.
(18) Wang, X.; Liao, Q.; Kong, Q.; Zhang, Y.; Xu, Z.; Lu, X.; Fu, H. *Angew. Chem.* **2014**, *126*, 5973; *Angew. Chem., Int. Ed.* **2014**, *53*, 5863.
(19) Xu, Z.; Liao, Q.; Shi, Q.; Zhang, H.; Yao, J.; Fu, H. *Adv. Mater.* **2012**, *24*, OP216.
(20) Zhang, C.; Zou, C. L.; Yan, Y.; Hao, R.; Sun, F. W.; Han, Z. F.; Zhao, Y. S.; Yao, J. *J. Am. Chem. Soc.* **2011**, *133*, 7276.
(21) Kang, L.; Fu, H.; Cao, X.; Shi, Q.; Yao, J. *J. Am. Chem. Soc.* **2011**, *133*, 1895.
(22) Zhang, X.; Zhang, X.; Zou, K.; Lee, C. S.; Lee, S. T. *J. Am. Chem. Soc.* **2007**, *129*, 3527.
(23) Liu, H.; Cao, X.; Wu, Y.; Liao, Q.; Jimenez, A. J.; Wurthner, F.; Fu, H. *Chem. Commun.* **2014**, *50*, 4620.
(24) Wang, Y.; Fu, H.; Peng, A.; Zhao, Y.; Ma, J.; Ma, Y.; Yao, J. *Chem. Commun.* **2007**, *16*, 1623.
(25) Kabe, R.; Nakanotani, H.; Sakanoue, T.; Yahiro, M.; Adachi, C. *Adv. Mater.* **2009**, *21*, 4034.
(26) Wei, L.; Yao, J.; Fu, H. *ACS Nano* **2013**, *7*, 7573.
(27) Kang, L.; Wang, Z.; Cao, Z.; Ma, Y.; Fu, H.; Yao, J. *J. Am. Chem. Soc.* **2007**, *129*, 7305.
(28) Lei, Y.; Liao, Q.; Fu, H.; Yao, J. *J. Phys. Chem. C* **2009**, *113*, 10038.
(29) Huang, L.; Liao, Q.; Shi, Q.; Fu, H.; Ma, J.; Yao, J. *J. Mater. Chem.* **2010**, *20*, 159.
(30) Winn, D.; Doherty, M. F. *AIChE J.* **2000**, *46*, 1348.
(31) Chandrasekhar, N.; Basak, S.; Mohiddon, M. A.; Chandrasekar, R. *ACS Appl. Mater. Interfaces* **2014**, *6*, 1488.
(32) Chandrasekar, R. *Phys. Chem. Chem. Phys.* **2014**, *16*, 7173.
(33) Kéna-Cohen, S.; Forrest, S. R. *Nat. Photonics* **2010**, *4*, 371.
(34) Tamboli, A. C.; Haberer, E. D.; Sharma, R.; Lee, K. H.; Nakamura, S.; Hu, E. L. *Nat. Photonics* **2007**, *1*, 61.
(35) Chen, R.; Ling, B.; Sun, X. W.; Sun, H. D. *Adv. Mater.* **2011**, *23*, 2199.
(36) Yoon, S. M.; Lee, J.; Je, J. H.; Choi, H. C.; Yoon, M. *ACS Nano* **2011**, *5*, 2923.
(37) O'Carroll, D.; Lieberwirth, I.; Redmond, G. *Nat. Nanotechnol.* **2007**, *2*, 180.
(38) Chen, R.; Van Duong, T.; Sun, H. D. *Sci. Rep.* **2012**, *2*, 244.